New Directions in Multi-Wavelength Astrophysics: Using Radio Data to Uncover Properties of Star-Forming Galaxies in the Young Universe

Katarzyna Małek[1·2], Darko Donevski[1·3], Mahmoud Hamed[1], Junais[1], Krzysztof Lisiecki[4] and Gabriele Riccio[1]

1. National Centre for Nuclear Research, Pasteura 7, 02-093 Warsaw, Poland
2. Aix Marseille Univ, CNRS, CNES, LAM, Marseille, France
3. SISSA, Via Bonomea 265, 34136 Trieste, Italy
4. Institute of Astronomy, Nicolaus Copernicus University in Torun, Grudziądzka 5, 87-100 Torun, Poland

Understanding how galaxies form their stars through cosmic time is one of the main topics in modern astrophysics. Nowadays, we have far-infrared and radio surveys that detect emission from millions of regular star-forming galaxies at the epoch of cosmic noon and beyond. Combining those unique data with optical and near-infrared surveys creates an opportunity to study star formation processes in the young Universe on a wide scale. In the last two years, a unique opportunity to perform a large-volume statistical investigation of star formation in evolving galaxies became possible due to the joint project of the Herschel Extragalactic Legacy Survey (HELP) and the International Low Frequency Array (LOFAR) survey. Multiwavelength data confirmed that far-infrared emission and thermal radio emission are excellent indicators of star-formation activity, while LOFAR radio data are crucial to understand how the addition of low-frequency radio spectra influences our estimates of galaxy star-formation rates. At the same time, both datasets are essential components in the broadband spectral energy modelling process, and using them together can give new quality in the galaxy evolution studies.

1 Introduction

A galaxy is a highly complicated mixture of stars, dust, and gas. Properties of all the ingredients and characteristics of the nature of the analyzed galaxy are displayed by the shape of its spectral energy distribution (hereafter SED). Specific wavelength ranges of the SED are responsible for different galaxy properties. Some of the properties are highly vivid on the SED, like, for example, the presence of the powerful active galactic nucleus (hereafter AGN) or the strength of the Polycyclic Aromatic Hydrocarbons (PAHs) in the mid-infrared (MIR) range of the spectra. With the technical developments, ground-based telescopes with better resolution and space instruments started to probe the sky at different parts of the electromagnetic spectrum. These observations allowed us not only to distinguish new galaxy populations but also to identify new properties of already known objects. Far-infrared (hereafter FIR) space-based telescopes, and high-resolution ground-based radio observations unveiled entirely hidden (or only partially visible in the optical observations) features of galaxies previously covered by dust.

1.1 What can the SED tell us about star-forming galaxies?

Most known galaxies were only observed in the ultraviolet (hereafter UV), optical and NIR wavelengths. Emission observed in that range originates from the stellar populations in the galaxy, which means that it provides information on the stellar content, age of stars, metallicity, etc. Generally speaking, the detailed star formation history (hereafter SFH) can be deduced from the stellar spectra of the galaxy itself. To decode this information, a combination of different stellar population synthesis models (i.e. Leitherer et al., 1999; Bruzual & Charlot, 2003; Maraston, 2005; Vazdekis et al., 2010), at a given spectral type, fixed metallicity and age, are used together to obtain the exact shape of the stellar SED, matching the observations. The UV part of the spectrum is emitted mainly by hot, blue stars and conveys the information on the young stellar population located in a galaxy. Colder evolved stars shape the optical part of the stellar spectra. During continuous star formation (SF) processes, the ratio between UV and optical spectrum remains rather constant because of the regular input of young massive stars. Only NIR fluxes rise as the NIR end of the stellar SED contains evolved and older stars in the galaxy. For that reason, the ratio between UV, optical and NIR fluxes, and in general, the shape of the stellar spectra, provides information if the SF process is still ongoing in the galaxy, or runs down or even finally stops. Thus, population synthesis models are used to calculate, for example, the stellar mass of a galaxy (mainly from the NIR range) or to estimate the star formation rate (SFR), from the blue end of the spectra. This method is weighted with uncertainties from the measurements or the theories behind the synthesis models. For instance, the estimation of the stellar mass of the galaxy can change by $\sim$50% while using different calculations for the thermally pulsing asymptotic giant branch stars, TP-AGB (Maraston et al., 2006; Bruzual, 2007; Tonini et al., 2009). Other uncertainties include the age–metallicity degeneracy (i.e. Worthey, 1994; Ferreras & Silk, 2000) or the dust attenuation law used for the SED fitting (i.e. Małek et al., 2018; Buat et al., 2019; Małek et al., 2020; Hamed et al., 2021).

The emission from the combination of the stellar spectra can be largely affected by dust attenuation. The dust distributed in the galaxy not only attenuates and deforms the light from different stellar populations in a galaxy but also reprocesses the attenuated light and re-emits the energy in the infrared (IR) wavelengths (Calzetti et al., 1994; Calzetti et al., 2000; Charlot & Fall, 2000). The dust attenuation is much stronger for the shorter wavelengths than for the longer ones and decreases beyond 0.5 μm (Charlot & Fall, 2000; Lo Faro et al., 2017). Therefore, the strength of dust attenuation is the limiting factor for the capability of using only stellar emission to calculate the SFR of the galaxy. Additional information on the SFR is hidden inside the dust emission, which is more difficult to detect than the optical one.

The presence of AGN in galaxies also contributes to the total energy emitted in the SED and to the variation of a galaxy's SF activity (both positively and negatively). Characteristic features that can help hunt hidden AGN in the host galaxy are mainly located in the NIR and MIR ranges of wavelength[1]. This part of the spectrum is only partially affected by the dust attenuation and shows mostly the emission from the large molecules of PAHs for star-forming galaxies (SFGs). For AGNs, the NIR-MIR emission originates from the dust torus and direct emission from the central AGN and also shows the scattering component (i.e. Fritz et al.,

[1]For Type 1, AGN features are also visible in the UV range.

2006; Alonso-Herrero et al., 2011; Ciesla et al., 2015; Stalevski et al., 2016).

Longer wavelengths (FIR) are dominated by the emission of cold dust heated by young, massive stars. Therefore this wavelength range possesses all the necessary information about the SFR in the galaxy. Having only FIR measurements, we are not able to calculate the stellar mass of the galaxy, as we do not probe all the evolved stars, but we can trace the SFR with very good precision. To increase the exactness of the SFR estimation, joint information from the UV/optical and FIR wavelengths should be taken into account. Adding observations in the submillimeter range, which traces the emission from the interstellar medium (molecular and atomic gas), sharpens up the complete picture of galaxy properties.

Those properties are widely used for the modelling of the SED of galaxies. Proper modelling, which takes into account galaxy properties at different wavelengths, can result in the estimation of the fundamental physical properties of galaxies, such as the stellar mass, SFR, dust luminosity, AGN contribution, and attenuation. This panchromatic view, which considers all possible broadband measurements spanning from the UV to the submillimeter range of the electromagnetic spectrum, is nowadays the main tool to understand the main physical properties of galaxies. However, this process is extremely challenging while only restricted information is taken into account – different types of galaxies can have a similar shape of SED in the restricted wavelength range (see for example Boquien et al., 2019). For example, building SEDs of a quiescent and a star-forming galaxy, based on the optical data only, can result in similar SEDs and estimated physical properties.

1.2 Panchromatic view of galaxies

The panchromatic analysis of galaxies and the Bayesian modelling of their full SED has become an important and widely used tool to understand galaxy evolution (i.e., Conroy, 2013; Buat et al., 2015; Donevski et al., 2020; Negrello et al., 2020; Thorne et al., 2021). Recent years have brought a lot of new data, like for example the *Herschel* Extragalactic Legacy Project[2] (HELP, Shirley et al., 2019, 2021), which provides a homogeneous, multi-wavelength catalogue from UV to FIR of millions of sources at wide redshift (hereafter z) range. The HELP catalogue is a unique dataset to test different physical properties, develop new SED software modules but also to prepare the pipeline for future surveys, as for example, the upcoming Legacy Survey of Space and Time (LSST) data from the Vera C. Rubin Observatory. For instance, Riccio et al. (2021), using the UV to FIR data from the HELP catalogue, have found that although LSST will provide very deep and accurate measurements in the optical, its short wavelength range covers only the evolved population of stars at low z. This will not allow us to properly estimate the SFR for those objects. This work is another proof that incomplete galaxy measurements can result in inaccurate estimations of their main physical properties. Moreover, thanks to the new and improved deblending software, `XID+`, which can help reduce FIR maps properly (Hurley et al., 2017; Pearson et al., 2018), it was possible to include more detailed models of AGN properties in the analysed host galaxies (Stalevski et al., 2016; Boquien et al., 2019; Yang et al., 2020; Ramos Padilla et al., 2022).

[2] `https://herschel.sussex.ac.uk/`

1.3 Adding the low-frequency radio spectra to refine the SFR estimates

Although FIR data contain information about the hidden SFR and partially about the AGN activity, it is not the only long wavelength range necessary to understand the physics of SFGs. Radio data, which carry information about synchrotron emission, can also be used to analyse both AGNs and SF regions in galaxies. Most of the visible brightest sources at radio wavelengths are derivatives of massive black holes at the centre of galaxies. However, the faint radio waves are also emitted from the ongoing SF regions in average, not highly active, galaxies. Synchrotron emission in SFGs is powered by high-energy electrons and positrons accelerated by supernova explosions – the remnants of supernova increase the density of cosmic ray electrons and accelerate them. At the same time, the same process amplifies the strength of the turbulent magnetic field of the galaxy (Tabatabaei et al., 2017). A very detailed description of the source of radio emission in galaxies can be found in Condon (1992). The power of the synchrotron emission in SFGs is closely related to their recent SFH, as both Type Ib and Type II supernovae are derived from massive, young stars. To summarise, in the radio range, we can see even better the hidden SF activity, and the imprint of newborn stars in the galaxy.

A remarkably tight correlation of the radio SED of SFGs with the IR luminosity has been observed at several radio bands across five orders of magnitude in luminosity (i.e., Helou et al., 1985; Condon, 1992; Yun et al., 2001; Calistro Rivera et al., 2017). This so-called FIR-radio correlation is often parametrized by the $q_{\rm IR}$ parameter, defined as a ratio of the total dust luminosity ($L_{\rm dust}$, usually calculated between 8 and 1 000 μm) and the radio luminosity at a given radio frequency:

$$q_{\rm IR} = \log\left(\frac{L_{\rm dust}}{L_{\nu,\rm radio} \times 3.75 \times 10^{12}\ \rm Hz}\right). \quad (1)$$

In the literature the most popular radio frequencies used for this equation are 21 cm, 150 MHz etc. The factor 3.75×10^{12} Hz is the frequency corresponding to 80 μm used to normalize the relation.

Unfortunately, the physical processes behind this tight correlation are poorly understood. The LOFAR project (van Haarlem et al., 2013) opens then a new window for SFG studies at low radio frequencies. The state-of-the-art radio telescope, characterized with unprecedented sensitivity and resolution, uncovered SF regions in distant galaxies, hidden behind dense clouds of dust.

Shimwell et al. (2019) published the first data release of the LOFAR Two-metre Sky Survey (LoTSS). This catalogue contains mosaicked images covering 424 square degrees and an extracted catalogue of 326 000 sources[3]. This catalogue was cross-matched with the multi-wavelength HELP database, among others, and 70% of those radio sources were associated with an optical/IR counterpart and photometric redshifts. This unique dataset opens a new path in the panchromatic view of SFGs and can improve understanding of the $q_{\rm IR}$ correlation. One of the most important open questions is whether $q_{\rm IR}$ evolves at high-z (e.g. $z > 2$) in different galaxy populations. Recent studies found dependencies of this relation on various galaxy parameters such as galaxy morphology (Molnár et al., 2018), stellar mass (i.e., Bonato et al., 2021; Delvecchio et al., 2021) or galaxy merging stage (Donevski

[3]The LOTSS catalogue is complete to 0.35 mJy for point sources.

& Prodanović, 2015). On top of this, previous studies, as for example Delhaize et al. (2017) and Calistro Rivera et al. (2017), provided constraints on the evolution of $q_{\rm IR}$ with z, finding a mild but significant decline that is yet to be fully understood. The multi-wavelength SED modeling can resolve some of the issues, e.g. by quantifying the level of potentially hidden AGN contribution. This will help better calibrate the radio emission as an SFR marker in the distant Universe.

2 How do radio data change our view on already known galaxies?

To illustrate the influence of the radio data on the SFR estimation and the AGN features, we selected 1 585 radio detected galaxies from the ELAIS N1 field, with a narrow redshift range ($0.65 < z < 0.75$). All galaxies have optical and FIR counterparts (*Herschel*). Photometric measurements, as well as photometric redshift estimation and the LOFAR fluxes detected at 150 MHz, were selected from the first data release of the LoTSS Deep Fields[4]. The detailed description of the radio dataset can be found in Sabater et al. (2021), the multi-wavelength data and source association are described by Kondapally et al. (2021), and the corresponding photometric redshifts by Duncan et al. (2021).

In our analysis, we used UV data from *GALEX* observations. The broadband u-band data were obtained using the MegaCAM instrument on the Canada-France-Hawaii Telescope. We have also used optical data (g, r, i, z, y, and the narrow-band NB921) from the Hyper-Suprime-Cam Subaru instrument. The NIR J and K band data were collected with the WFCAM on the UK Infrared Telescope, while four MIR bands data, 3.6, 4.5, 5.8 and 8.0 μm, were detected by the IRAC instrument onboard the *Spitzer* Space Telescope. FIR fluxes were obtained from *Herschel* PACS and SPIRE maps from the HELP catalogue (Shirley et al., 2021).

2.1 *Modelling with an improved* CIGALE V2022.0 *tool*

We modelled all the selected radio-detected galaxies with CIGALE V2022.0 (Yang et al., 2022) - the new, improved version of the X-CIGALE SED software tool (Yang et al., 2020) which itself is an updated version of CIGALE (Boquien et al., 2019), a broadband SED fitting code based on the energy balance principle. To build the radio component CIGALE V2022.0 uses both thermal (in the NEBULAR module) and synchrotron component (RADIO module) calculated with the $q_{\rm IR}$ parameter with the default value equal to 2.58 and a free parameter which describes the slope of the power-law synchrotron emission, $\alpha_{\rm SF}$. Moreover, CIGALE V2022.0 allows to define the radio-loudness parameter for AGN, $R_{\rm AGN}$, defined as a ratio between AGN luminosities measured at 5 GHz and at 2500Å, and then the slope of the power-law AGN radiation (assumed isotropic). This flexibility makes CIGALE V2022.0 an efficient tool to analyse physical properties of multiwavelength survey data from X-ray to radio wavelengths (Yang et al., 2022).

To build the stellar component of radio-selected galaxies, we used the stellar population synthesis models by Bruzual & Charlot (2003) with the initial mass function given by Chabrier (2003) and we also included the module. We used a simple delayed SFH. The energy emitted from massive, young stars was attenuated according to the recipe of Charlot & Fall (2000). We followed the dust emission

[4] `https://lofar-surveys.org/deepfields.html`

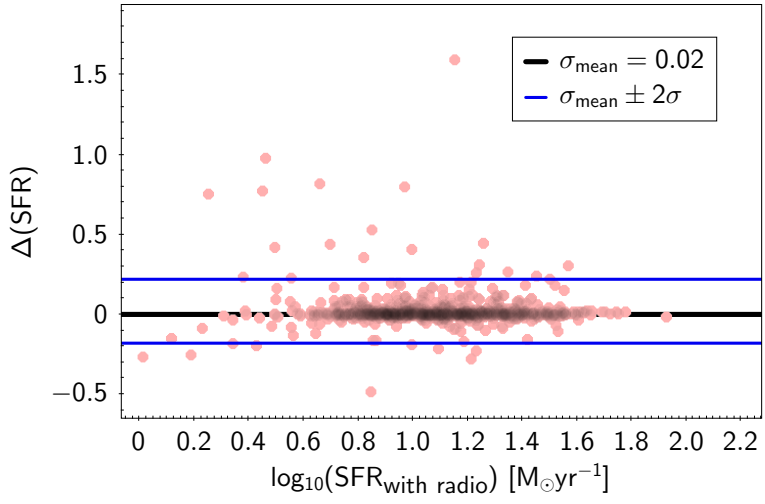

Fig. 1: The distribution of ΔSFR of all SF galaxies as a function of $\log_{10}$(SFR) averaged over the last 100 Myr [$\mathrm{M}_\odot\mathrm{yr}^{-1}$] calculated with the full photometric coverage from UV to the radio. The thick black line represents the mean value of the ΔSFR ($\sigma_{\rm mean}$), while two thin blue lines limit the area of the 2σ distributions.

templates given by Dale et al. (2014). We have also included the AGN component described in Stalevski et al. (2016), and the improved radio module (Yang et al., 2020).

2.2 Results

To check the influence of radio data on the estimated SFR of galaxies, we ran CIGALE v2022.0 twice - once with radio data and the radio module, and once without them. For the final analysis, we selected from both runs only the galaxies with a good fit to the observational data, using $\chi^2_{\rm red}$ and $\chi^2_{\rm IR\ red}$ parameters[5], with both values lower than 2.5. We have also selected only galaxies with $\log_{10}$(SFR) larger than 0 to remove all quiescent galaxies. This selection results in a 934 SFGs (69% of the selected sample) with very good fits, either with or without radio data, which allows us to compare possible differences in the estimated SFR. We calculated the ΔSFR as a difference of two SFR in the logarithmic scale. Then we ran CIGALE v2022.0 with RADIO module but without FIR data, to check if radio data can sufficiently recover SFR in galaxies (Figs. 2c and 2f). We have found an excellent agreement between all runs, shown in Fig. 3. The scatter found for the run without FIR data is much larger than for the run with radio data, but the general behaviour is very encouraging.

We have found that SFR estimated with and without radio data gives similar results with mean ΔSFR equal to 0.020, which does not suggest any biases in our estimations. We have calculated σ value of the ΔSFR distribution (σ=0.10) and

[5]The $\chi^2_{\rm red}$ is a quantity calculated as a reduced value of χ^2 for the whole SED fit, while the $\chi^2_{\rm IR\ red}$ represents recalculated value of $\chi^2_{\rm red}$ for $\lambda > 8$ μm, which represents the threshold between stellar and dust spectrum of the galaxy. Detailed description can be found in Małek et al. (2018).

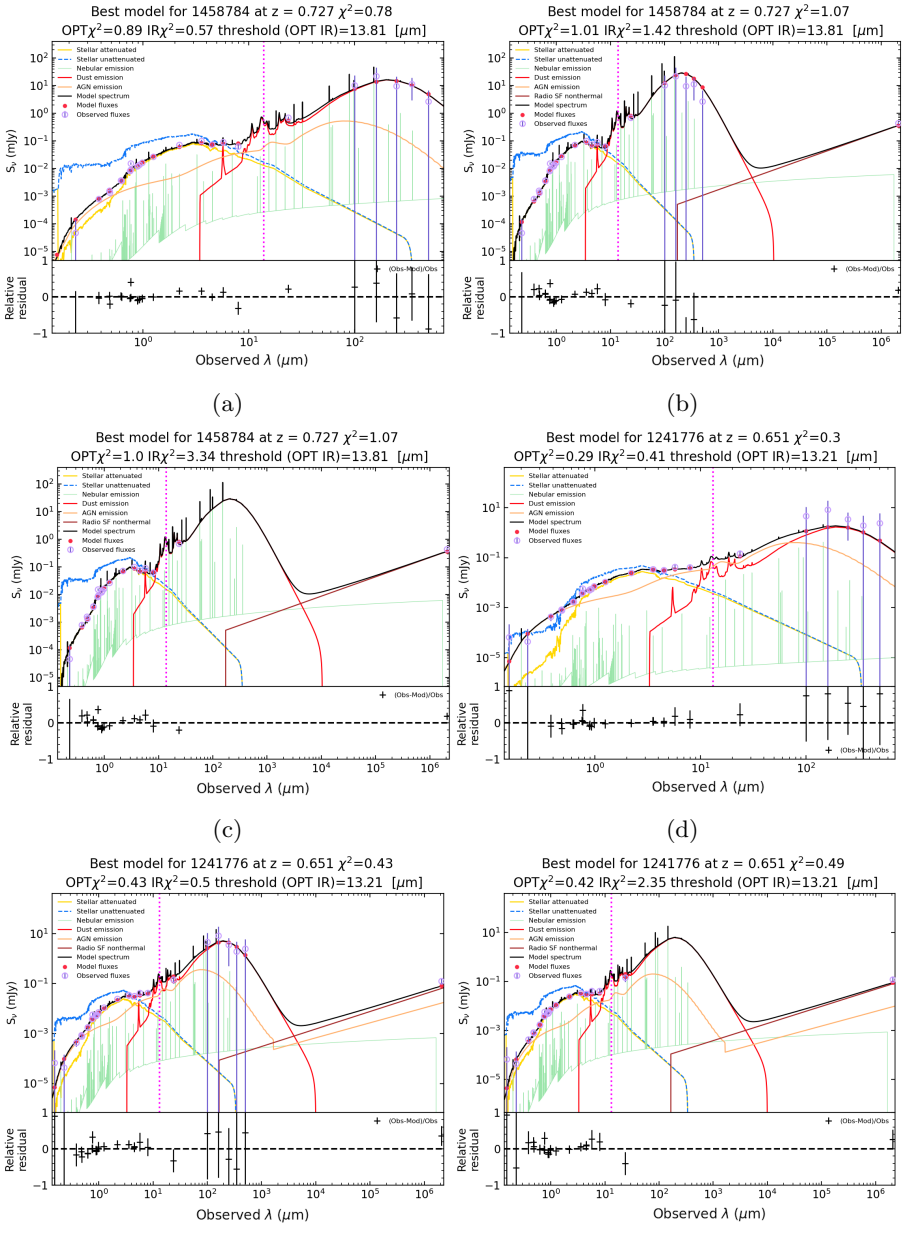

Fig. 2: Two examples of galaxy fitting procedures performed in this work. Two galaxies are presented in a), b), c) and in d), e) f) panels respectively. In both cases the ΔSFR value for them is larger than 0.3. First column shows SED fits without radio data and radio component, while the middle one presents full SED fitting from UV to radio. The last column shows SED fitting results with radio data and radio component but without FIR data. Observed fluxes are plotted with open violet squares. Filled red circles correspond to the model fluxes. The final model is plotted as a solid black line. The solid green line shows a nebular spectrum. The remaining three lines correspond to the stellar, dust, and AGN components.

we performed a visual check of objects outside the 2σ region. Figure 2 shows two examples of fitted galaxies with and without radio components and also without FIR data (last column). The calculated ΔSFR for the first galaxy was found to be 0.31. We have found that the main difference between both fits is the $\mathrm{AGN_{frac}}$. The $\mathrm{AGN_{frac}}$ estimated for the full UV-radio SED fitting equals to 0.00 ± 0.04, while the same quantity estimated for the UV-FIR SED is larger (0.08 ± 0.15). The $\log_{10}$ SFR estimated for the full SED fit and the fit without radio data is 1.57 ± 0.10 [$\mathrm{M_\odot yr^{-1}}$] and 1.26 ± 0.46 [$\mathrm{M_\odot yr^{-1}}$], respectively. What is very motivating, the SFR calculated without FIR data, and based only on the UV/optical and radio data, is very close to SFR estimated with the full photometric information, and equals 1.42 ± 0.09 [$\mathrm{M_\odot yr^{-1}}$]. In the second case, the $\mathrm{AGN_{frac}}$ and $\log_{10}$ SFR estimated for the full UV-radio SED fitting equals to 0.25 ± 0.12, and 0.50 ± 0.59, respectively. The same values for the UV-FIR estimation only are calculated as 0.35 ± 0.13 and 0.07 ± 1.49. In the case of the estimated $\log_{10}$ SFR without FIR, but with radio, the calculated value is equal to 0.51 ± 0.66. Those results show a very important role of radio data and radio modules to estimate real SFR in galaxies.

We conclude that the radio data can help to better estimate the AGN component and correct the SFR obtained from the broadband SED fitting by kind of deblending AGN luminosity from the SF regions.

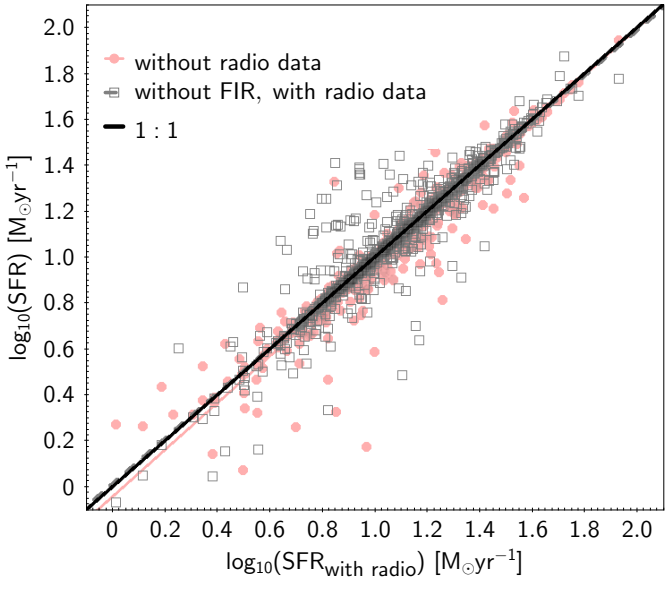

Fig. 3: The comparison between $\log_{10}(\mathrm{SFR_{with\ radio}})$ obtained from the total UV–radio fitting and the same values estimated without the radio component (pink dots) and with radio data and the radio component but without FIR data (gray open squares). The solid black line represents the 1:1 relation. Pink and olives lines behind the black line are linear fits to the data.

3 Conclusions

Star formation is usually mostly obscured by dust, covering our view when we look with optical telescopes. The radio waves, similarly to infrared wavelengths, penetrate the dust allowing us to obtain a complete picture of galaxy SF. With FIR data, radio can guarantee a new level of SFR estimation using the broadband SED fitting method. Detailed study of radio detection and the inclusion of radio measurements to panchromatic galaxy study can lead to a more accurate estimation of SFR and AGN activity. Adding radio data to the broadband SED fitting software brings new challenges and makes the SED fitting even more panchromatic than before. Moreover, detailed but statistical study of radio-detected galaxies at high redshift can uncover new hints on SF in the young universe.

Acknowledgements. This research was supported by the Polish National Science Centre under SONATA BIS grants UMO-2018/30/E/ST9/00082 and UMO-2020/39/D/ST9/00720.

References

Alonso-Herrero, A., et al., *ApJ* **736**, 2, 82 (2011)

Bonato, M., et al., *A&A* **656**, A48 (2021)

Boquien, M., et al., *A&A* **622**, A103 (2019)

Bruzual, G., in A. Vallenari, R. Tantalo, L. Portinari, A. Moretti (eds.) From Stars to Galaxies: Building the Pieces to Build Up the Universe, *ASP Conference Series*, volume 374, 303 (2007)

Bruzual, G., Charlot, S., *MNRAS* **344**, 4, 1000 (2003)

Buat, V., et al., *A&A* **577**, A141 (2015)

Buat, V., et al., *A&A* **632**, A79 (2019)

Calistro Rivera, G., et al., *MNRAS* **469**, 3, 3468 (2017)

Calzetti, D., Kinney, A. L., Storchi-Bergmann, T., *ApJ* **429**, 582 (1994)

Calzetti, D., et al., *ApJ* **533**, 682 (2000)

Chabrier, G., *PASP* **115**, 809, 763 (2003)

Charlot, S., Fall, S. M., *ApJ* **539**, 2, 718 (2000)

Ciesla, L., et al., *A&A* **576**, A10 (2015)

Condon, J. J., *ARA&A* **30**, 575 (1992)

Conroy, C., *ARA&A* **51**, 1, 393 (2013)

Dale, D. A., et al., *ApJ* **784**, 1, 83 (2014)

Delhaize, J., et al., *A&A* **602**, A4 (2017)

Delvecchio, I., et al., *A&A* **647**, A123 (2021)

Donevski, D., Prodanović, T., *MNRAS* **453**, 1, 638 (2015)

Donevski, D., et al., *A&A* **644**, A144 (2020)

Duncan, K. J., et al., *A&A* **648**, A4 (2021)

Ferreras, I., Silk, J., *MNRAS* **316**, 4, 786 (2000)

Fritz, J., Franceschini, A., Hatziminaoglou, E., *MNRAS* **366**, 767 (2006)

Hamed, M., et al., *A&A* **646**, A127 (2021)

Helou, G., Soifer, B. T., Rowan-Robinson, M., *ApJL* **298**, L7 (1985)

Hurley, P. D., et al., *MNRAS* **464**, 885 (2017)

Kondapally, R., et al., *A&A* **648**, A3 (2021)

Leitherer, C., et al., *ApJS* **123**, 1, 3 (1999)

Lo Faro, B., et al., *MNRAS* **472**, 2, 1372 (2017)

Małek, K., et al., *A&A* **620**, A50 (2018)

Małek, K., et al., in K. Małek, M. Polińska, A. Majczyna, G. Stachowski, R. Poleski, Ł. Wyrzykowski, A. Różańska (eds.) XXXIX Polish Astronomical Society Meeting, volume 10, 221–225 (2020)

Maraston, C., *MNRAS* **362**, 3, 799 (2005)

Maraston, C., et al., *ApJ* **652**, 1, 85 (2006)

Molnár, D. C., et al., *MNRAS* **475**, 1, 827 (2018)

Negrello, M., et al., *PASA* **37**, e025 (2020)

Pearson, W. J., et al., *A&A* **615**, A146 (2018)

Ramos Padilla, A. F., et al., *MNRAS* **510**, 1, 687 (2022)

Riccio, G., et al., *A&A* **653**, A107 (2021)

Sabater, J., et al., *A&A* **648**, A2 (2021)

Shimwell, T. W., et al., *A&A* **622**, A1 (2019)

Shirley, R., et al., *MNRAS* **490**, 1, 634 (2019)

Shirley, R., et al., *MNRAS* **507**, 1, 129 (2021)

Stalevski, M., et al., *MNRAS* **458**, 3, 2288 (2016)

Tabatabaei, F. S., et al., *ApJ* **836**, 2, 185 (2017)

Thorne, J. E., et al., *MNRAS* **505**, 1, 540 (2021)

Tonini, C., et al., *MNRAS* **396**, 1, L36 (2009)

van Haarlem, M. P., et al., *A&A* **556**, A2 (2013)

Vazdekis, A., et al., *MNRAS* **404**, 4, 1639 (2010)

Worthey, G., *ApJS* **95**, 107 (1994)

Yang, G., et al., *MNRAS* **491**, 1, 740 (2020)

Yang, G., et al., *ApJ* **927**, 2, 192 (2022)

Yun, M. S., Reddy, N. A., Condon, J. J., *ApJ* **554**, 2, 803 (2001)